Enhanced light absorption in thin film silicon solar cells with Fourier-series based periodic nanostructures

Xiaowei Guo,[1,*] Dashuai Wang,[1] Bang Liu,[1] Shaorong Li,[1] and Xing Sheng[2]

[1]*School of optoelectronic information, University of Electronic Science and Technology, Chengdu, 610054, China*
[2]*Department of Electronic Engineering, Tsinghua University, Beijing, 100084, China*
[*]*gxw@uestc.edu.cn*

Abstract: We proposed a Fourier-series based periodic nanostructure(FSPN) for light trapping in thin film silicon solar cells. By globally optimizing the Fourier coefficients across entire silicon absorption spectrum, we obtained a FSPN structure with short circuit current density greater than 24 mA/cm^2 for a 1μm real silicon absorption layer. The spectral analysis shows at normal incidence the FSPN exhibits a collection effect of periodic gratings and performs over 84.6% better than random texture. The angular analysis shows that the FSPN outperforms grating and random textures within 70 °.

OCIS codes: (040.5350) Photovoltaic; (350.4238) Nanophotonics and photonic crystals.

References and links

1. A. V. Shah, H. Schade, M. Vanecek, J. Meier, E. Vallat-Sauvain, N. Wyrsch, U. Kroll, C. Droz, and J. Bailat, "Thin-film silicon solar cell technology," Prog. Photovolt. Res. Appl. **12**(23), 113–142 (2004).
2. J. Müller, B. Rech, J. Springer, and M. Vanecek, "TCO and light trapping in silicon thin film solar cells," Sol. Energy **77**(6), 917–930 (2004).
3. L. Zeng, P. Bermel, Y. Yi, B. A. Alamariu, K. A. Broderick, J. Liu, C. Hong, X. Duan, J. Joannopoulos, and L. C. Kimerling, "Demonstration of enhanced absorption in thin film Si solar cells with textured photonic crystal back reflector," Appl. Phys. Lett. **93**(22), 221105 (2008).
4. M. A. Green and S. Pillai, "Harnessing plasmonics for solar cells," Nat. Photonics **6**(3), 130–132 (2012).
5. C. Battaglia, C. M. Hsu, K. Söderström, J. Escarré, F. J. Haug, M. Charrière, M. Boccard, M. Despeisse, D. T. Alexander, M. Cantoni, Y. Cui, and C. Ballif, "Light trapping in solar cells: can periodic beat random," ACS Nano **6**(3), 2790–2797 (2012).
6. E. Yablonovitch and G. D. Cody, "Intensity enhancement in textured optical sheets for solar cells," IEEE Trans. Electron. Dev. **29**(2), 300–305 (1982).
7. Z. Yu, A. Raman, and S. Fan, "Fundamental limit of light trapping in grating structures," Opt. Express **18**(S3 Suppl 3), A366–A380 (2010).
8. X. Sheng, S. G. Johnson, J. Michel, and L. C. Kimerling, "Optimization-based design of surface textures for thin-film Si solar cells," Opt. Express **19**(S4 Suppl 4), A841–A850 (2011).
9. V. Ganapati, O. D. Miller, and E. Yablonovitch, "Light trapping textures designed by electromagnetic optimization for sub-wavelength thick solar cells," IEEE J. Photovoltaics **4**(1), 175–182 (2014).
10. C. Haase and H. Stiebig, "Thin-film silicon solar cells with efficient periodic light trapping texture," Appl. Phys. Lett. **91**(6), 061116 (2007).
11. E. D. Palik, *Handbook of Optical Constants of Solids* (Acadmic Press, 1985).
12. V. Liu and S. Fan, "S4: A free electromagnetic solver for layered periodic structures," Comput. Phys. Commun. **183**(10), 2233–2244 (2012).
13. R. Dewan, V. Jovanov, S. Hamraz, and D. Knipp, "Analyzing periodic and random textured silicon thin film solar cells by Rigorous Coupled Wave Analysis," Sci. Rep. **4**, 6029 (2014).
14. J. Oh, H. C. Yuan, and H. M. Branz, "An 18.2%-efficient black-silicon solar cell achieved through control of carrier recombination in nanostructures," Nat. Nanotechnol. **7**(11), 743–748 (2012).
15. R. Chriki, A. Yanai, J. Shappir, and U. Levy, "Enhanced efficiency of thin film solar cells using a shifted dual grating plasmonic structure," Opt. Express **21**(S3 Suppl 3), A382–A391 (2013).

#253989 Received 18 Nov 2015; revised 25 Dec 2015; accepted 27 Dec 2015; published 19 Jan 2016

1. Introduction

Thin-film Si solar cells offer many advantages, including a lower cost, potential for high efficiency with lower material quality, and use of smaller quantities of silicon. However, it is difficult to maintain competitively high efficiencies in conventional bulk cells while shrinking the volume of silicon available to absorb incident photons. On the other hand, as an indirect bandgap material, silicon photovoltaics are handicapped by poor absorption in the near-infrared wavelengths, which becomes particularly problematic for thin devices and can lead to unacceptable photocurrent loss [1]. Effective photon management can address this issue and holds the promise of realizing ultrahigh-efficiency thin cells at low cost. As a successfully demonstrated strategy, use of photonic structures becomes essential in thin cells. Various photonic structures have been proposed as top or bottom textures to confine electromagnetic energy in the device to increase absorption, including random structures [2], back Bragg reflectors [3], metallic nanoparticles [4], and periodic nanostructures [5]. To predict light absorption enhancement(AE), Yablonovitch established the Lambertian models from a ray-optics perspective in which under the key assumptions of isotropic scattering, for an ideal random texture, the AE factor has an upper limit of πn in 1D or $4n^2$ in 2D for a film (with index n) of infinite thickness and spectral range at normal incidence [6]. When the cell thickness is reduced comparable to or smaller than the wavelength of interest, the wave effects of light become prominent. Yu et al. developed a statistical temporal coupled mode theory formalism to describe light AE, and demonstrated that, for grating, the Lambertian limit can be exceeded but with significant angular dependency [7]. To overcome the angular dependency, Sheng et al. proposed a periodic structure based on mathematical Fourier series(FSPN) as back scatter and numerically obtained a AE larger than the Lambertian limit at the wavelength of 900nm [8]. In 2013, Ganapati et al. demonstrated such structures perform roughly 30% better than randomly textured structures in the wavelength range of 750nm to 860nm, but they fall short of the Lambertian limit of $4n^2$ [9]. However, both calculations were based on a weak absorber with fixed refractive index and constant absorption coefficient, which can't reflect real light trapping performance. In [8] the silicon layer was assumed with a refractive index of 3.6 and absorption coefficient of 12.56 cm^{-1}, while in [9] the weak absorber was set with a refractive index of 3.5 and absorption coefficient of 1600 cm^{-1}.

In this paper, we proposed a FSPN on top of a real silicon absorber and calculated the AE across entire silicon absorption spectrum from 300nm to 1100nm. In second section, we briefly introduced the construction of FSPN. In third section, the global optimization of the FSPN was described, and in forth section, the optimized results and discussion were made.

2. Fourier-series based periodic nanostructures

In principle, any arbitrarily shaped periodic texture, described by the function *f(x,y)*, can be represented by a Fourier series:

$$f(x,y)=\sum_{m=-\infty}^{\infty}\sum_{n=-\infty}^{\infty}C_{mn}e^{j(\frac{2m\pi x}{\Lambda}+\frac{2n\pi y}{\Lambda})} \tag{1}$$

Where Λ is the periodicity, and C_{mn} are the Fourier coefficients with the orders of m and n. It is evident that an ideal random texture can be achieved when the periodicity is infinity, and C_{mn}, m and n are more enough. On the other hand, a planar film is described when all the coefficients are set to zero.

From Eq. (1), we observe that the component is cosine or sine function so that the FSPN can be formed by interference lithography, a low-cost large-area fabrication technique. To avoid small highly resonant features that would not be robust in fabrication, it is necessary to truncate the Fourier series. Considering the fabrication feasibility, the first 5 orders were

#253989 Received 18 Nov 2015; revised 25 Dec 2015; accepted 27 Dec 2015; published 19 Jan 2016

determined as degrees of freedom including DC components. Due to limited computing ability, we only consider one dimension case as below:

$$f(x) = C_0 + \sum_{i=1}^{4} (a_i \cos\frac{2i\pi x}{\Lambda} + b_i \sin\frac{2i\pi x}{\Lambda}) \quad (2)$$

Where a_i and b_i are the Fourier coefficients. Obviously, the texture profile is determined by the periodicity and the Fourier coefficients. We have demonstrated there is almost no difference in light trapping between the optimized textures with only cosine or sine components and those with both components. Therefore, Eq. (2) is further reduced to:

$$f(x) = C_0 + \sum_{i=1}^{4} (a_i \cos\frac{2i\pi x}{\Lambda}) \quad (3)$$

3. Optimization method

The basic solar cell devices used in our numerical model originate from [10] that are illustrated in Fig. 1. From top to bottom, it consists of transparent conductive oxide (TCO), crystalline silicon (c-Si), and a perfect electric conductor on the backside. The bottom interface between silicon and reflector is flat, and only the top interface between Si and TCO is textured. As a consequence, parasitic plasmonic losses of the metal back contact were not considered. For the sake of simplicity, the silicon was considered to be intrinsic and the effects of p and n regions were neglected. The TCO material was set to Zinc oxide with 500nm thickness and its optical constants used for this study were obtained from [10]. The optical constants of silicon were extracted from handbook of optical constants [11]. The random and grating textures were introduced for comparison purpose. All the texture thicknesses(from peak to valley) were set to be identical for fair comparison. Under the textures, the thickness of the silicon layer is constant with 1μm. For comparison purpose, TCO absorption loss was not considered. Optical simulations are based on the Rigorous Coupled-Wave Analysis (RCWA) technique which is a fast and efficient technique to analyze the light propagation in thin-film devices with nanotextured interfaces [12]. It has been demonstrated that when the texture thickness is within 500nm the RCWA approach provides the simulation accuracy [13].

The surface textures were optimized by maximizing the short circuit current density J_{sc} over the entire silicon absorption spectrum (300nm-1100nm) if we assume that all the electron-hole pairs contribute to the photocurrent,

$$J_{SC} = \frac{q}{hc} \int \lambda \cdot A(\lambda) \cdot I_{AM1.5G}(\lambda) d\lambda \quad (4)$$

where q is the elementary charge, λ is the incident wavelength, h is Planck constant, c is the speed of light, $A(\lambda)$ is the silicon absorption spectrum and $I_{AM1.5G}(\lambda)$ is the incident AM1.5G solar spectral irradiance. The absorption of the silicon absorber layer can be expressed as $A(\lambda) = 1 - R(\lambda)$.

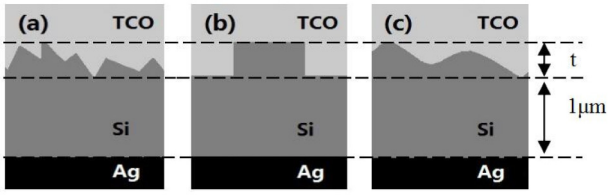

Fig. 1. Schematic illustration of surface textures in a basic solar cell. (a), (b) and (c) correspond to the random, grating and FSPN textures, respectively.

#253989 Received 18 Nov 2015; revised 25 Dec 2015; accepted 27 Dec 2015; published 19 Jan 2016

According to Yu model [7], one can obtain large AE at specific wavelength comparable to the grating periodicity. For FSPN, the periodicity should be set to make most sub-periodicities Λ/i located within the silicon absorption spectrum. The overlapping of multiple AEs generates a large absorption increase. As a result, the FSPN periodicity is at least larger than 600nm for 4 orders, which leads us to choose the periodicity starting from 700nm in global optimization. By changing the Fourier coefficients (a_1, a_2, a_3, a_4), one can optimize the FSPN profile by maximizing J_{sc}. In our optimization, the coefficients are integers.

4. Results and discussion

Figure 2 shows the optimized structure parameters and J_{sc} corresponding to each periodicity at different thicknesses and incidence angles. In Fig. 2(b) with 300nm thickness case, the periodicity varies from 700nm to 1400nm. It can be seen at each periodicity there is an optimized texture. For example, the optimized coefficients associated with the periodicity of 1400nm are (0, 0, 3, 0), as shown under the curves. It is noted that all the associated J_{sc} exhibits similar and its variation is less than 8%. At normal incidence, the J_{sc} at 1400nm periodicity is 24.11 mA/cm^2, while the planar structure obtains a J_{sc} of 13.60 mA/cm^2. There is 84.6% increase in J_{sc} using FSPN. Under oblique incidence, the averaged J_{sc} decreases. For 30° incidence, the averaged J_{sc} is about 0.82 mA/cm^2 lower than that at normal incidence. When the angle switches to 60°, the averaged J_{sc} decrease with a value of 5.32 mA/cm^2.

From Figs. 2(a) and 2(c), we observe that the relation between J_{sc} and periodicity keeps similar to that in Fig. 2(b), but the tendency is that all J_{sc} shift up with the increase of thickness. For 100nm thickness [Fig. 2(a)], the averaged J_{sc} is 20.31 mA/cm^2, while at 500nm thickness [Fig. 2(c)] the averaged J_{sc} is improved to 26.33 mA/cm^2. It is emphasized that the J_{sc} increase magnitude is far below the thickness increase, which indicates the absorption is dominated by the texture profile that enlarges the optical path. For large texture thickness, however, there results in more loss of photogenerated carriers because of Auger recombinations [14]. On the other hand, there is less feasibility in fabrication of such high-aspect-ratio nanostructures. Therefore, choice of 300nm texture thickness for light trapping is better. Since the optimized J_{sc} are similar for all periodicities, choice of either periodicity is possible for real use. However, large periodicity allows large resonant features, which benefits its fabrication. For example, if the target periodicity is 1400nm, then the smallest sub-periodicity is 1400/4 = 350nm, which adapts well to the fabrication ability for UV light interference lithography. In contrast, the smallest sub-periodicity is 175nm when selecting 700nm periodicity. Thus, selecting 1400nm periodicity is obviously preferable.

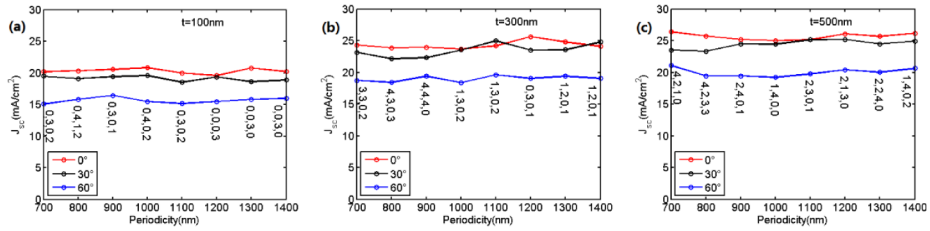

Fig. 2. Optimized coefficients and J_{sc} at different texture periodicities and incident angles. (a), (b) and (c) correspond to the texture thickness of 100nm, 300nm, 500nm, respectively.

To verify the effectiveness of the presented RCWA approach, we calculated these J_{sc} using a finite element method(FEM). The FEM results are slightly higher than RCWA ones. At 300nm and 500nm thicknesses, the J_{sc} errors are about 0.67 mA/cm^2 and 1.31 mA/cm^2, which accords wells with the results in [13] and thus provides the accuracy of the RCWA simulations. Figure 3 plotted the electric field distribution in grating and FSPN textured devices at 400nm, 700nm and 1000nm wavelengths. In both cases, the periodicities are 1400nm. In Figs. 3(a), 3(d) and 3(g) corresponding to the planar devices, it can be seen that

#253989 Received 18 Nov 2015; revised 25 Dec 2015; accepted 27 Dec 2015; published 19 Jan 2016

most of the energy resides outside the silicon absorption layer. By using the grating texture [Figs. 3(b), 3(e) and 3(h)], the light energy is partly coupled into the absorption layer. It is noted in Fig. 3(b) the incoupled energy is fully absorbed by the silicon layer due to large absorption coefficient at 400nm wavelength. At long wavelengths, weak absorption causes strong electric field distribution and thus large AE can be obtained. In FSPN textured devices illustrated in Figs. 3(c), 3(f) and 3(i), more light energy enters the silicon layer. The electric field distribution exhibits uniform and stronger in the silicon layer. Especially, at 1000nm wavelength, the electric field inside outperforms that outside the absorption layer, indicating great absorption improvement.

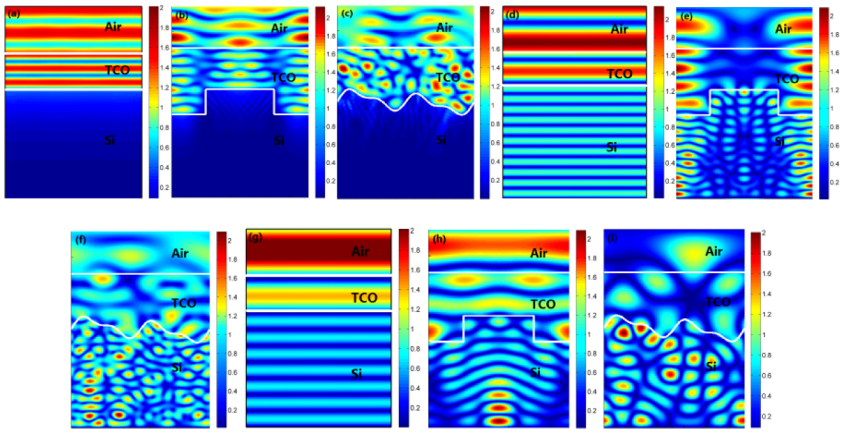

Fig. 3. Electric field distributions across the basic Si solar cell structure at 400nm [Figs. 3(a)-3(c)], 700nm [Figs. 3(d)-3(f)], and 1000nm [Figs. 3(g)-3(i)] wavelengths with normal incidence.

In the following, we analyzed the performance of the FSPN texture with 1400nm periodicity and compared with conventional random and grating textures. The random texture data was extracted from [13] in which Asahi U-type glass was measured by an atomic force microscope. For gratings, the periodicities were set to same as the sub-periodicities of FSPN, that is, 1400nm, 700nm, 466nm, and 350nm. The grating geometry is rectangular and its duty cycle is 1:1. All the texture thicknesses were fixed to 300nm.

Figure 4 presents the spectral response for FSPN at normal incidence. In Fig. 4(a), it can be seen that random textured device behaves better than the bare planar one in entire silicon absorption spectrum. The gratings further enhance the light absorption, but different periodicities perform differently [see Fig. 4(b)]. It is also evident that the FSPN and gratings surpass the Lambertian limit at long wavelengths. For clarification, we smoothed the texture curves, as plotted in Fig. 4(c). For 350nm periodicity, the absorption is relatively narrow but reaches peak at 450nm wavelength. With the increase of the grating periodicity, the absorption window becomes wider, and the absorption falls short of the random data at short wavelengths. The periodicities of 466nm and 700nm result in large AE at long wavelengths. However, the FSPN is superior to either one, exhibiting a collection effect of single gratings, which results in its absorption window wider than grating and random textures. It is also noted that at short wavelengths the light loss comes mainly from the reflection at the interfaces. Due to the small penetration depth for blue light, a light trapping effect is negligible [13]. The FSPN shows better anti-reflection performance. From 300nm to 550nm wavelengths, the FSPN exhibits 20% higher than the grating with 700nm periodicity. After 550nm wavelengths, the weak absorption nature of silicon comes to emerge, where the light trapping of the FSPN texture plays the vital role and thus the AE quickly increase with wavelength. In the inset of Fig. 4(c), we plotted AE of the FSPN defined by the absorption divided by single absorption [8]. In the region of 750-860nm wavelength Ganapati et al.

#253989 Received 18 Nov 2015; revised 25 Dec 2015; accepted 27 Dec 2015; published 19 Jan 2016

studied, the AEs for FSPN are inferior to the Lambertian limit, while their results are higher than the Lambertian limit [9]. At 900nm wavelength Sheng et al used, our result shows the AE is also lower than the Lambertian limit, whereas their result is slightly greater than the Lambertian limit [8]. The discrepancies should ascribe to use different absorbers and optimized structures. Around 870nm, 930nm, and 1010nm wavelengths, the AEs outperform the Lambertian limit.

The angular response for FSPNs is illustrated in Fig. 5. Figure 5(a) gives the angle-averaged AE against the Lambertian limit [9]. At the wavelengths below 900nm, the angle-averaged AE is inferior to the Lambertian limit. Over 900nm, the angle-averaged AEs at some wavelengths provide potential to surpass the Lambertian limit. To compare the FSPN and gratings, the J_{sc} versus incidence angle is shown in Fig. 5(b). Like the spectral response, periodic gratings perform better than random texture, while the FSPN outperforms the gratings within 70°. For angles up to ~80°, current enhancement is observed as compared to the planar case. Within 40°, the J_{sc} is enhanced by a factor of 1.85, which is over 1.7 for optimized dual grating with an angle tolerance of 15° [15]. Even within 80°, the J_{sc} are over 10 mA/cm^2, superior to the pyramid array in a μc-Si device with same configuration in which only 10 mA/cm^2 was numerically obtained [10]. Finally, it is worth mentioning that the J_{sc} will decrease if the absorption loss in TCO is considered.

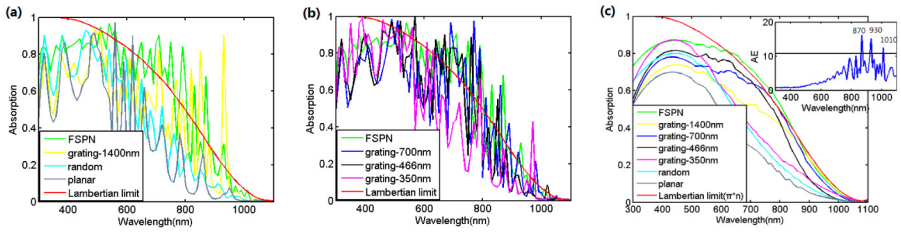

Fig. 4. Spectral response for the FSPN texture. (a) and (b) present light absorption for all the textures. To distinguish the difference, (c) gives the smoothed curves. The inset illustrates AEs for the FSPN texture.

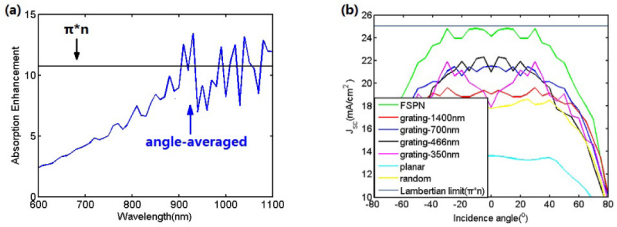

Fig. 5. Angular response for the FSPN texture. (a) means angle-averaged AE for the FSPN texture and (b) J_{sc} for all the textures.

5. Conclusion

Through global optimization, we achieved a FSPN that exhibits broadband and wide angular absorption as compared to conventional random and grating textures. The FSPN can be easily fabricated by interference lithography if the Fourier series are reasonably truncated. It is probable to achieve broader and wider absorption by adoption of 2D FSPNs. Also, it is possible to obtain larger absorption if using decimal coefficients for optimization.

Acknowledgment

This work was supported by the Science-Technology Foundation of Sichuan Province, China(No. 2014HH0068).

#253989 Received 18 Nov 2015; revised 25 Dec 2015; accepted 27 Dec 2015; published 19 Jan 2016